Comunicações Geológicas

Comunicações Geológicas (2026) 113, 1, 31-40
ISSN: 0873-948X; **e-ISSN:** 1647-581X

Magnetic characterization of non-geological materials: implications on human health

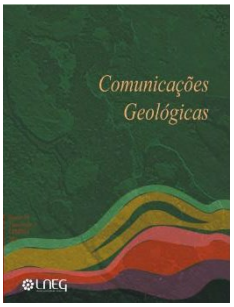

Caracterização magnética de materiais não geológicos: implicações na saúde humana

D. Sá[1], C. Cruz[1,2*], H. Sant'Ovaia[1,2]

DOI: https://doi.org/10.34637/rd5y-p387
Recebido em 06/03/2026 / Aceite em 21/07/2026
Publicado online em setembro de 2026

Original article
Artigo original

Abstract: This study investigates the magnetic properties of commonly used non-geological materials and evaluates their potential implications for human health. The analyzed materials include tobacco and its by-products (filters and ashes), industrial paints, hair dyes and developer, garage dust, fuel soot and metal scarps. A multi-analytical approach combining optical microscopy, scanning electron microscopy with energy-dispersive spectroscopy (SEM-EDS), X-ray fluorescence (XRF), and magnetic techniques (magnetic susceptibility, χ, isothermal remanent magnetization, IRM, and thermomagnetic curves, K/T) was applied to identify and characterize iron-bearing phases. Iron oxides were detected in several materials, particularly tobacco, ashes, used filters, fuel soot, garage dust and metal scraps. Tobacco ash and fuel soot samples contained ultrafine iron-rich particles (~2 µm), which are small enough to be inhaled, penetrate pulmonary alveoli, and potentially enter the bloodstream. In contrast, industrial paints and hair dyes displayed predominantly diamagnetic behavior, excluding significant iron oxide presence. The results demonstrate that everyday materials and combustion-derived residues may act as sources of ultrafine ferromagnetic particles with potential health implications. These findings highlight the importance of magnetic characterization as a complementary tool in environmental and biomedical studies aimed at assessing exposure to iron-rich particulate matter.

Keywords: SEM/EDS, geochemical analyses, optical observations, iron oxides, magnetic studies.

Resumo: Este estudo investiga as propriedades magnéticas de materiais não geológicos frequentemente usados no quotidiano, incluindo tabaco e os seus subprodutos (filtros e cinzas), tintas industriais, tintas para cabelo e oxidante, poeiras de garagem, fuligem de combustível e aparas metálicas. Foi aplicada uma abordagem multianalítica que combinou técnicas de microscopia (Lupa binocular, Microscópio Eletrónico de Varrimento – Espectroscopia de Dispersão de Energia, MEV-EDS), análise química por fluorescência de raios X (FRX) e caracterização magnética (suscetibilidade magnética, χ; Magnetização Remanescente Isotérmica, MRI; e curvas termomagnéticas, K/T), para identificar óxidos de ferro em várias amostras. Tabaco, cinzas, filtros, fuligem, poeiras de garagem e aparas metálicas apresentaram partículas magnéticas, sendo que as cinzas e a fuligem exibiram partículas ultrafinas (~2 µm) capazes de ser inaladas e de entrar na corrente sanguínea através dos alvéolos pulmonares. Em contraste, as tintas industriais e as tintas para cabelo mostraram um comportamento diamagnético, excluindo a presença significativa de óxidos de ferro. Os resultados destacam que a exposição a materiais do quotidiano pode representar riscos para a saúde devido às partículas ferromagnéticas ultrafinas, sublinhando a relevância da caracterização magnética em contextos ambientais e biomédicos.

Palavras-chave: MEV/EDS, análises geoquímicas, observações óticas, óxidos de ferro, estudos magnéticos.

[1] Department of Geosciences, Environment and Spatial Planning, Faculty of Sciences of Porto University, Rua do Campo Alegre, 4169-007 Porto, Portugal.
[2] Institute of Earth Sciences, Rua do Campo Alegre, 4169-007 Porto, Portugal.

* Corresponding author / Autor correspondente: d_r_sa@hotmail.com

1. Introduction

This study focuses on the identification of magnetic particles in common materials and evaluates their potential impact on human health. Materials analyzed include tobacco and its by-products (filters and ashes), hair dyes and developer, industrial paints, fuel soot (diesel and gasoline), garage dust and metal scraps from a cutting workroom. These substances are widely used or encountered daily, making their characterization relevant for environmental and biomedical research.

The presence of magnetite in human tissues was first reported over 30 years ago (Kirschvink *et al*., 1992), with implications for cerebral function due to its redox activity and strong ferromagnetism. Abnormal concentrations of magnetite and other iron oxides have been associated with neurodegenerative diseases such as Alzheimer's and Parkinson's (Fischer *et al*., 1997; Loeffler *et al*., 1995), as well as epilepsy (Ikeda, 2001), strokes, anemia, and certain cancers (Haacke *et al*., 2005). Magnetic minerals are easily assimilated in the lungs during breathing (Cohen, 1973), and fine magnetic particles have been correlated with respiratory and cardiovascular diseases (Samet *et al*., 2000). Cigarette combustion has been linked to increased health risks due to its complex biomass composition (Baliga *et al*., 2003; Calderón-Garcidueñas *et al*., 2019; Gunawan *et al*., 2024; Maher, 2019). Combustion occurs across three thermal zones: pre-combustion (100 – 200 ºC), burning (700 – 950 ºC), and ash formation (200 – 600 ºC) (Baker, 1987).

The size of iron (Fe) particles is a critical factor, as they must not exceed a maximum diameter of 2 µm to pose a significant risk to human health. Particulate matter within this micrometric scale

can penetrate the pulmonary alveolar barriers (Dezube, 2023) and enter the bloodstream. Once in circulation, these particles can be transported by ferritin, a protein responsible for iron storage and transport (Umbreit *et al*., 2002; Simovich *et al*., 2003), allowing them to accumulate in internal organs and potentially leading to the development of the previously cited diseases.

The objective of this work is to identify and characterize magnetic particles present in these materials and assess their role as potential risk to the human health. By providing this initial magnetic characterization, the study contributes to a better understanding of everyday exposure, offering data that may support future public health discussions and consumer awareness. To achieve this, a multi-analytical approach combining microscopy, chemical analysis and magnetic characterization was employed.

The methodological approach applied in this study demonstrates the relevance of environmental magnetism within Earth Sciences, particularly for the investigation of anthropogenic materials and pollution-related processes. Magnetic techniques such as magnetic susceptibility (χ), isothermal remanent magnetization (IRM), and thermomagnetic analyses (K/T) are widely used in geosciences to identify iron-bearing minerals, evaluate mineralogical transformations, and trace environmental contamination. By extending these methodologies to non-geological materials, this study shows how approaches traditionally applied to soils, sediments, and rocks can also be used to characterize combustion-derived particles and urban contaminants associated with human activities. The integration of electron microscopy with energy-dispersive spectroscopy (SEM-EDS) and X-ray fluorescence (XRF,) and magnetic measurements provides a robust multi-analytical framework capable of identifying ultrafine iron-rich particles and linking them to specific combustion and mechanical processes. The detection of ultrafine magnetic particles in tobacco ashes, fuel soot, garage dust, and metallic residues demonstrates the applicability of environmental magnetic methods to urban and environmental monitoring studies. Consequently, the methodology adopted in this work reinforces the importance of environmental magnetism as a geoscientific tool for assessing anthropogenic contamination and its potential implications for environmental and human health.

2. Materials and methods

A total of 50 samples were prepared in 8 cm³ cubes, with approximately 3 replicates per material (Fig. 1, Table 1). The dataset included thirteen hair dye samples of different colors and developer (used to activate the color), five samples of industrial paints, eight samples of tobacco, four tobacco ash samples, eight tobacco filters samples, three garage dust samples, six fuel soot samples, and four metal scraps samples (Tab. 1). To obtain soot from the exhaust pipes of both gasoline and diesel vehicles, a piece of cotton was used and subsequently stored in 8 cm³ cubes. Preparation methods varied according to analytical requirements: samples such as garage dust and all the materials from workroom underwent magnetic separation using ferrite magnets to extract magnetically susceptible components. The samples that were subjected to thermomagnetic curve analysis, such as tobacco ash and tobacco samples were ground with a manual agate grinding mill to obtain homogeneous fine particles, while all the others were manually separated to isolate the finer fractions. The samples that were subjected to IRM analysis, such as, used tobacco filter, tobacco ash and tobacco samples were also ground with a manual agate grinding mill. These specific materials were selected for IRM and thermomagnetic analyses because they represent the primary focus of this exploratory study, exhibiting the most significant magnetic signals and potential for mineralogical transformation during combustion.

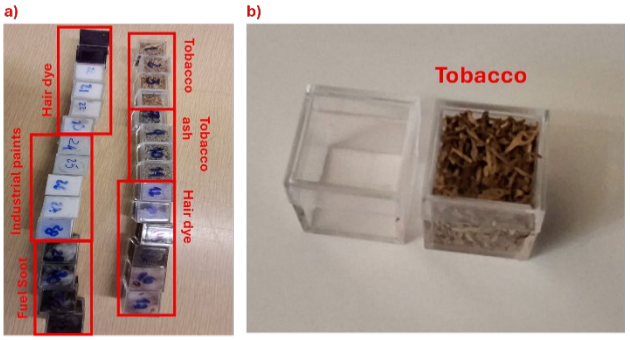

Figure 1. a) Analyzed samples on the study storage in cubes; b) plastic cube used to transport and analyze the samples.

Figura 1. a) Amostras analisadas no estudo armazenadas em cubos; b) cubo plástico utilizado para transporte e análise das amostras.

A multi-analytical approach was employed to characterize these materials. Optical observations were performed with a LEICA DFC295 binocular magnifying glass equipped with a digital camera to identify particle morphology; this equipment is from *Departamento de Geociências, Ambiente e Ordenamento de Territorio* (DGAOT) of the *Faculdade de Ciências da Universidade do Porto* (FCUP). Scanning electron microscopy (SEM-EDS) was conducted using a FEI Quanta 400 FEG ESEM coupled with an energy-dispersive spectroscopy detector to

Table 1. Samples under study and techniques used on each sample (×– not performed; ✓ – performed). SEM: Scanning Electron Microscopy- Energy Dispersive Spectroscopy, XRF: X-ray fluorescence; χ: Magnetic susceptibility; IRM: Isothermal remanent magnetization; K/T: Thermomagnetic curves.

Tabela 1. Amostras em estudo e técnicas utilizadas em cada amostra (×– não realizada; ✓ – realizada). MEV: Microscopia Eletrônica de Varrimento - Espectroscopia de Energia Dispersiva; XRF: Fluorescência de raios X; χ: Suscetibilidade magnética; MRI: Magnetização remanescente isotérmica; K/T: Curvas termomagnéticas.

Sample	Type of material	Binocular microscope	SEM-EDS	XRF	Magnetic studies		
					χ	MRI	K/T
#1	Cigarette	✓	×	✓	✓	×	×
#2	Cigarette	×	×	✓	✓	×	×
#3	Cigarette	×	✓	✓	✓	×	×
#4	Cigarette	×	×	✓	✓	×	✓
#5	Cigarette	×	×	✓	✓	×	×
#6	Cigarette	×	×	✓	✓	✓	×
#7	Cigarette	✓	✓	✓	✓	×	×
#8	Cigarillo	✓	✓	✓	✓	✓	✓
#9	Tobacco ash	×	×	×	✓	×	×
#10	Tobacco ash	✓	✓	✓	✓	✓	×
Ci#13	Tobacco ash	×	×	×	×	✓	✓
Ci#2	Tobacco ash	×	×	×	×	×	✓
#13	Cigarette filter (used)	×	×	✓	✓	✓	×
#14	Cigarette filter (used)	×	×	✓	✓	×	×
#15	Cigarette filter (used)	×	×	×	✓	×	×
#16	Cigarette filter (used)	×	×	×	✓	×	×
#17	Cigarette filter (used)	×	×	×	✓	×	×
#18	Cigarette filter (used)	×	×	×	✓	×	×
#19	Cigarette filter (unused)	×	×	×	✓	×	×
#20	Cigarette filter (unused)	×	×	×	✓	×	×
#21	Private garage dust	×	×	×	✓	×	×
#22	Private garage dust	✓	✓	✓	✓	×	×
#23	Private garage dust	×	×	✓	✓	×	×
#24	Hair dye	×	×	✓	✓	×	×
#25	Hair dye	×	×	×	✓	×	×
#26	Hair dye	×	×	×	✓	×	×
#27	Hair dye	×	×	×	✓	×	×
#28	Hair dye	×	×	×	✓	×	×
#29	Hair dye	×	×	×	✓	×	×
#30	Hair dye	×	×	×	✓	×	×
#31	Hair dye	×	×	×	✓	×	×
#32	Hair dye	×	×	×	✓	×	×
#33	Hair dye	×	×	×	✓	×	×
#34	Hair dye	×	×	×	✓	×	×
#35	Hair dye	×	×	×	✓	×	×
#36	Developer	×	×	×	✓	×	×
#37	Industrial Paint (Grey)	×	×	×	✓	×	×
#38	Industrial Paint (Grey)	×	×	×	✓	×	×
#39	Industrial Paint (White)	×	×	×	✓	×	×
#40	Industrial Paint (White)	×	×	×	✓	×	×
#41	Gasoline Soot	✓	✓	✓	✓	×	×
#42	Gasoline Soot	×	×	✓	✓	×	×
#43	Gasoline Soot	×	×	✓	✓	×	×
#44	Diesel Soot	✓	✓	✓	✓	×	×
#45	Diesel Soot	×	×	✓	✓	×	×
#46	Diesel Soot	×	×	✓	✓	×	×
#47	Metal Workroom (Aluminum)	✓	×	✓	✓	×	×
#48	Metal Workroom (Iron)	✓	×	✓	✓	×	×
#49	Metal Workroom (Iron)	✓	×	✓	✓	×	×
#50	Metal Workroom (Mix)	✓	✓	✓	✓	×	×

examine morphology and chemical composition; this equipment belongs to *Centro de Materiais da Universidade do Porto* (CEMUP). Chemical composition was determined via X-ray fluorescence (XRF) using Oxford Instruments equipment, providing semi-quantitative elemental data; this equipment is from DGAOT-FCUP. Magnetic properties were studied through mass-normalized magnetic susceptibility (χ, expressed in 10^{-8} m³/kg), isothermal remanent magnetization (IRM), and thermomagnetic curve analysis (K/T). Mass-corrected susceptibility was measured with an Agico KLY-4S Kappabridge, with data processed in SUMEAN software, this equipment belongs to *Instituto de Ciências da Terra* (ICT). The magnetic susceptibility (χ) is the relationship between the magnetization induced (M) in a material and the external field (H) and is defined as $M=\chi H$. IRM measurements were performed by applying progressively increasing magnetic fields up to 1.8 T at room temperature, with acquisition curves decomposed using the Max UnMix algorithm (Maxbauer *et al*., 2016), and the equipment was from *Instituto Dom Luiz* (IDL). This technique is used to identify the ferromagnetic components of the sample based on the value of the saturation magnetic field (Robertson and France, 1994). The Max UnMix technique is a statistical tool used to decompose the magnetic properties of a material to identify the specific magnetic components within it. The process is based on analyzing magnetization curves, where Saturation Isothermal Remanent Magnetization (SIRM) represents the total magnetic capacity of the sample, essentially the maximum magnetic signal the sample can hold. Using the software, the contribution of each magnetic component is calculated, showing the percentage that each individual component represents relative to the total SIRM. To determine if a sample is dominated by low-coercivity minerals (easy to magnetize, like magnetite) or high-coercivity minerals (difficult to magnetize, like hematite), the S-ratio is used: values close to 1 indicate a dominance of low-coercivity minerals, while lower values suggest a significant presence of high-coercivity minerals (Thompson and Oldfield, 1986). The specific identification of each mineral is achieved through the coercivity, B1/2, which is the magnetic field strength required to reach 50% of a component's saturation, this value defines the magnetic "hardness" and acts as a fingerprint for the mineral. In the software, this parameter often appears as Log(B1/2), which is simply the B1/2 value converted to a logarithmic scale (log10) to make it easier to visualize different mineral types on the same plot. Finally, the Dispersion Parameter (DP) measures the variability of the grains within a single component: a low DP indicates that the mineral grains are very uniform in size and shape, while a high DP reveals a wide physical diversity among those grains. Together, these parameters allow to "unmix" the complex magnetic signature of a natural sample to understand its geological or environmental history.

Thermomagnetic analyses were conducted under low applied fields, recording susceptibility during heating and cooling cycles up to 600 °C to identify Curie temperatures of ferromagnetic phases, from IDL. This analysis was conducted using argon flux because argon replaces oxygen and prevents unwanted chemical reactions that could alter the sample's mineralogical or metallic composition during heating. This integrated methodology ensured robust identification of iron oxides and magnetic phases across diverse materials.

3. Results

3.1. Optical Observations

Binocular magnifying glass observations reveal distinct morphological features across materials (Fig. 2). Cigarette tobacco showed elongated, flattened particles (Fig. 2a), while cigarillo tobacco contained wider grains (Fig. 2b). Tobacco ashes (Fig. 2c) consisted of amorphous, homogeneous char material with variable particle sizes. Metal scraps included aluminum fragments larger than 1 mm with visible cutting directions, iron particles with heterogeneous morphologies and oxidation, and mixed alloys with diverse shapes and colors (Figs. 2d, e, f). Garage dust displayed rounded to sub-rounded grains of beige and grey tones, consistent with transport by tires, shoes, or wind (Fig. 2g). Fuel soot samples differed in staining intensity, gasoline soot produced lighter stains, whereas diesel soot-stained cotton more strongly, though individual particles were not distinguishable (Fig. 2h, 2i).

3.2. SEM/EDS Analyses

SEM observations confirmed the presence of iron in several materials. Cigarette tobacco contained Fe particles smaller than 1 µm (Fig. 3a) in different shapes, one being rounded and others angular, while cigarillo tobacco contained one larger particle approximately 200 µm (Fig. 3b). In addition to iron, aluminum (potentially hazardous to humans), magnesium (essential, but harmful in excess), and phosphorus (also essential, but toxic in

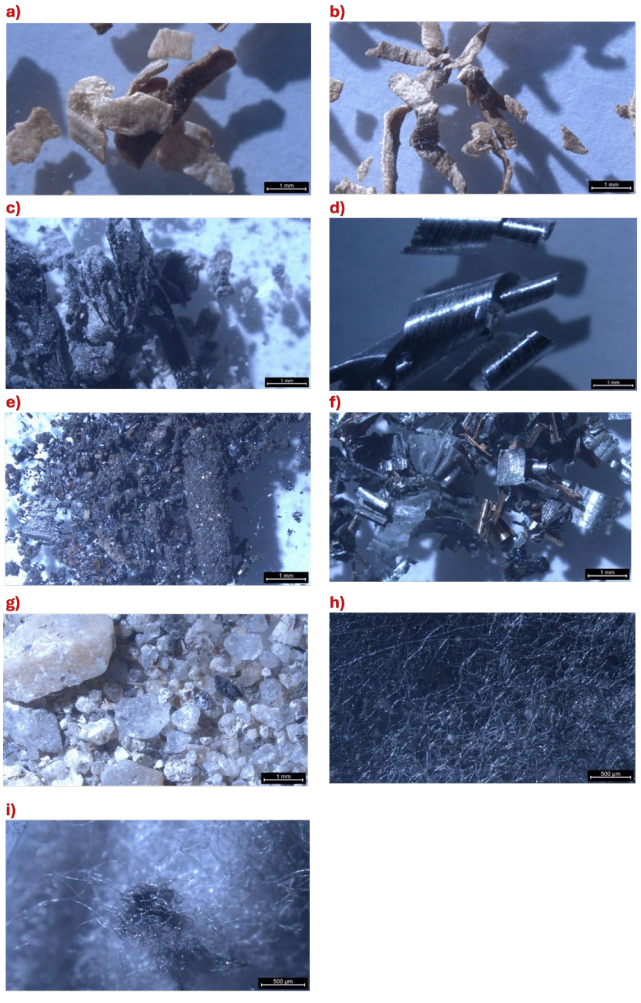

Figure 2. Optical observation of the materials. a) Cigarillo; b) cigarette; c) tobacco ash; d) aluminum from Workroom; e) iron from Workroom; f) mixture from Workroom; g) dust from the private garage; h) diesel soot; i) gasoline soot.

Figura 2. Observação ótica dos materiais. a) Cigarrilha; b) cigarro; c) Cinza de tabaco; d) alumínio da oficina; e) ferro da oficina; f) mistura me materiais da oficina; g) pó da garagem privada; h) fuligem gasóleo; i) fuligem de gasolina.

excess) were detected in tobacco samples. The cigarillo tobacco samples were like the cigarette tobacco samples; however, zinc was also found, which is likewise essential yet toxic in excessive amounts. Tobacco ashes revealed iron oxides below 2 µm (Fig. 3c). In the tobacco ashes, titanium and aluminum were found to be potentially toxic elements, and magnesium was also detected. In the garage dust samples, a concentration of 72.6% Fe was recorded. It is safe to say that these are iron oxides (Fig. 3d). In the diesel (Fig. 3e) and gasoline (Fig. 3f) soot samples, one Fe particle measuring approximately 1 µm was found. In the diesel soot, iron was detected in addition to titanium and sulfur. Metal scraps exhibited large Fe particles, often folded or mechanically broken (Fig. 3g) which indicates that in time they can break and be inhaled entering the human body. In the workroom material mixtures, iron, chromium, and aluminum were detected.

3.3. Geochemical Analyses (XRF)

The X-ray fluorescence (XRF) analytical results demonstrate that within the tobacco samples (Fig. 4a), potassium (K) is the predominant constituent, followed by calcium (Ca). Iron (Fe) ranks as the third most abundant element, exhibiting a mean value concentration of 1353 ppm (Tab. 2). Some other constituents (*e.g.*, mercury (Hg), manganese (Mn), copper (Cu), zinc (Zn), titanium (Ti), rubidium (Rb), and tin (Sn)) are classified as toxic heavy metals or hazardous elements upon inhalation, posing significant

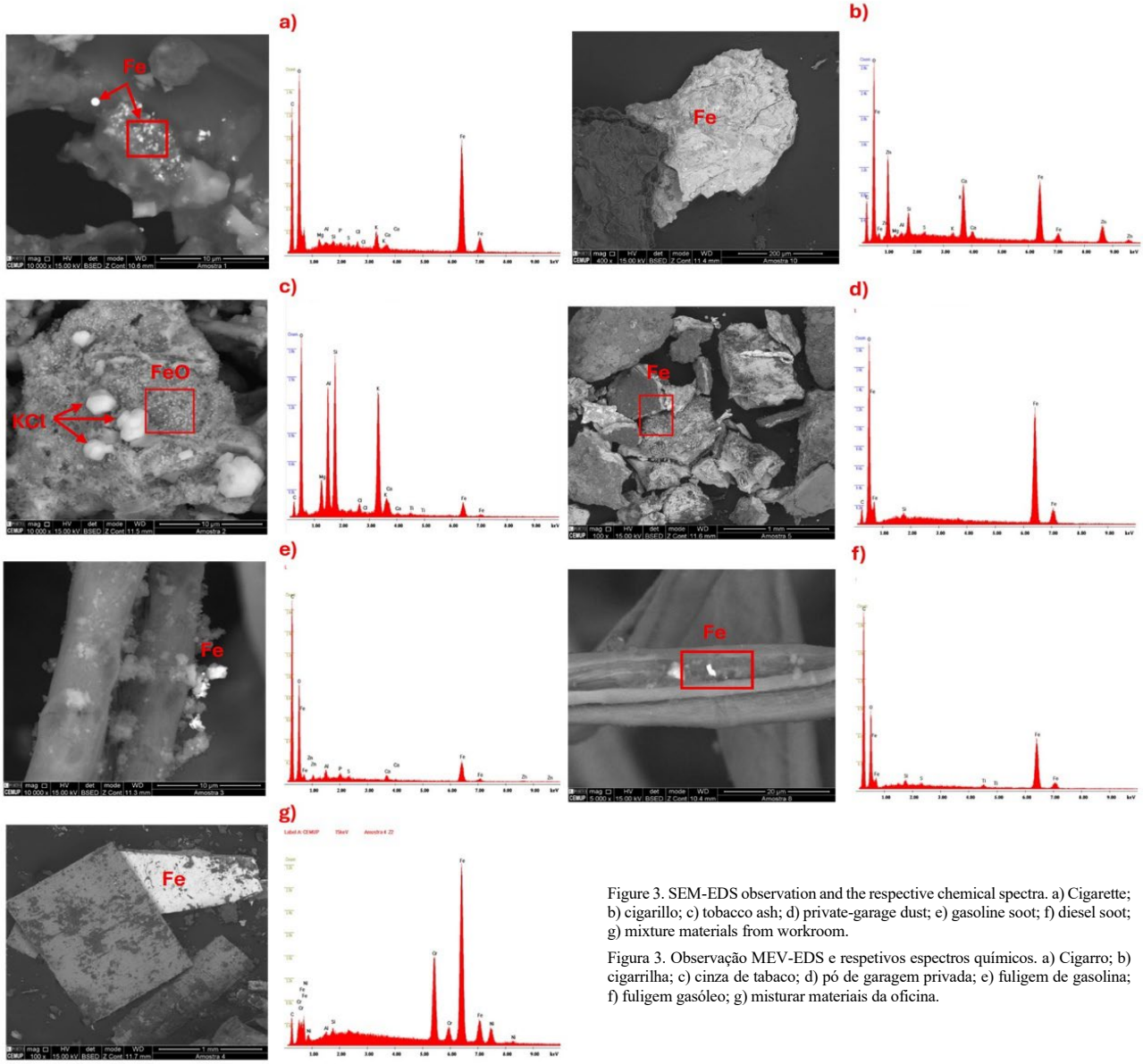

Figure 3. SEM-EDS observation and the respective chemical spectra. a) Cigarette; b) cigarillo; c) tobacco ash; d) private-garage dust; e) gasoline soot; f) diesel soot; g) mixture materials from workroom.

Figura 3. Observação MEV-EDS e respetivos espectros químicos. a) Cigarro; b) cigarrilha; c) cinza de tabaco; d) pó de garagem privada; e) fuligem de gasolina; f) fuligem gasóleo; g) misturar materiais da oficina.

Table 2. Results of x-ray fluorescence (XRF) and magnetic susceptibility (χ). Fe was the only element marked for XRF on this table. XRF expressed in ppm; χ expressed in m3/kg; Nd - Not detected.

Tabela 2. Resultados de fluorescência de raios X (FRX) e suscetibilidade magnética (χ). O Fe foi o único elemento marcado para FRX nesta tabela. FRX expresso em ppm; χ expresso em m3/kg; Nd - Não detetado.

Type of material	XRF (Fe) (ppm)	χ (x10^{-8} m^3/kg)
Tabacco	1353.43	3.78
Tabacco ash	2450.50	179.22
Cigarette filter (used)	Nd	0.81
Cigarette filter (unused)	Nd	-0.64
Garage dust	9860.67	253.22
Hair dye	Nd	-1.12
Industrial Paint (Gray)	Nd	0.09
Industrial Paint (White)	Nd	-0.28
Gasoline soot	252.33	10.436
Diesel soot	1302	22.69
Metal Workroom	378953.50	22267.11

physiological risks. The tobacco ash samples (Fig. 4b) exhibit the same elemental composition but generally display higher concentrations, with iron (Fe) in particular presenting a notably elevated mean value of 2450 ppm (Tab. 2). The used cigarette filter samples reveal a significantly limited elemental profile, containing only three detectable elements, calcium (Ca) as the most abundant, followed by potassium (K), and zinc (Zn). All identified elements in the filters (Fig. 4c) were found in trace or significantly lower quantities compared to the tobacco results, furthermore, iron (Fe) was notably not detected in these samples. Regarding the garage dust samples (Fig. 4d), the three predominant elements identified were calcium (Ca) as the primary constituent, followed by potassium (K), and iron (Fe), which exhibited a recorded mean value of 9861 ppm (Tab. 2). Additionally, the analysis detected the presence of other elements categorized as toxic substances, particularly when dispersed as inhalable particulate matter (*e.g.*, lead (Pb), manganese (Mn), copper (Cu), zinc (Zn), titanium (Ti), zirconium (Zr), rubidium (Rb), and strontium (Sr)).

Regarding the diesel soot (Fig. 4e) samples, calcium (Ca), iron (Fe), and potassium (K) represent the most abundant elements in descending order of concentration. Within this matrix, iron (Fe) exhibited a mean value of 1302 ppm. Furthermore, significant traces of elements with a high potential to be harmful (*e.g.*, zinc (Zn), strontium (Sr), and rubidium (Rb)). The gasoline soot samples (Fig. 4f) exhibit an initial elemental distribution like the garage dust, with the same three predominant elements. However, the recorded mean value for iron (Fe) was 757 ppm (Tab. 2). In addition to these primary constituents, some other materials with a toxicological risk when inhaled were registered (*e.g.*, zinc (Zn), rubidium (Rb), and strontium (Sr)).

The workroom samples are subdivided into three categories. In the iron-based samples (Fig. 4g), iron (Fe) is the dominant constituent with a substantial mean concentration of 378953 ppm (Tab. 2), followed by calcium (Ca) and chromium (Cr). This specific matrix also allows for the identification of other materials classified as toxic heavy metals or hazardous elements upon inhalation (*e.g.*, nickel (Ni), cobalt (Co), vanadium (V), manganese (Mn), copper (Cu), zinc (Zn, titanium (Ti), zirconium (Zr), potassium (K), rubidium (Rb), and tin (Sn)). In the aluminum-based samples (Fig. 4h), the three primary elements are, in descending order, copper (Cu) and iron (Fe), with a mean value of 4771 ppm, alongside registered traces of elements potentially toxic or hazardous once inhaled (*e.g.*, chromium (Cr), titanium (Ti), manganese (Mn), nickel (Ni), zinc (Zn), potassium (K), and calcium (Ca)). Finally, a mixture from workroom (Fig. 4i) was analyzed, where copper (Cu) was the most abundant element, followed by iron (Fe) with a mean value of 42291 ppm, and zinc (Zn). Other detectable elements in this mixture included lead (Pb), chromium (Cr), nickel (Ni), cobalt (Co), manganese (Mn), tin (Sn), molybdenum (Mo), and titanium (Ti).

It should be noted that all non-primary elements were detected at low concentrations, nonetheless, they pose severe health risks upon chronic exposure or inhalation. The average Iron (Fe) composition is marked on table 2.

3.4. Magnetic Susceptibility (χ)

Three distinct magnetic behaviors were identified. Diamagnetic responses were observed in unused filters (mean value: -0.643 × 10^{-8} m³/ kg), hair dyes (mean value: -1.12 × 10^{-8} m³/ kg), and white paints (mean value: -0.107 × 10^{-8} m³/ kg). Paramagnetic behavior characterized tobacco (mean value: 3.779 × 10^{-8} m³/ kg), used filters (mean value: 0.811 × 10^{-8} m³/ kg), fuel soot (mean value: 16.566 × 10^{-8} m³/ kg), and grey paints (mean value: 0.0915 × 10^{-8} m³/ kg). Ferromagnetic responses were found in tobacco ashes (mean value: 179.220 × 10^{-8} m³/ kg) and garage dust (mean value: 253.216 × 10^{-8} m³/ kg) (Tab. 2).

3.5. Isothermal Remanent Magnetization (IRM)

The IRM data (Tab. 3) were analyzed on tobacco, tobacco ash and used filters, and the unmixing of the magnetic components was performed using Max UnMix software (Maxbauer *et al.*, 2016).

We prioritized samples for IRM analyses based on a main criterion of the specific research goal of tracking the thermal transformation of iron phases during tobacco combustion. Due to the limited number of analytical slots available at the laboratory facility, we chose tobacco, tobacco ashes and filters since they were deemed the most representative for the study's core objectives.

Tobacco contained two components: magnetite (SIRM = 3.8 × 10^{-2} A/m) and, most likely, goethite (SIRM = 1.0 × 10^{-1} A/m; Fig. 5a; Tab. 3). Magnetite was identified as the primary magnetic mineral in the tobacco ashes (SIRM = 1.51 A/m) and used filters (SIRM = 2.20 × 10^{-2} A/m) (Fig. 5b and 5c, respectively; Tab. 3).

Table 3. Results of IRM (isothermal remanent magnetization) analysis for each sample, with parameters extracted from the demagnetization window. The values are presented for each identified magnetic component: S-ratio (parameter indicating the relative proportion of low-coercivity and high-coercivity materials), relative contribution (%), SIRM (isothermal remanent magnetization saturation, in A/m), log($B_{1/2}$) (half-remanence field, in mT), $B_{1/2}$ (mT), and DP (dispersion parameter, in mT).

Tabela 3. Resultados da análise MRI (magnetização remanescente isotérmica) para cada amostra, com parâmetros extraídos da janela de desmagnetização. Os valores são apresentados para cada componente magnético identificado: razão S (parâmetro que indica a proporção relativa de materiais de baixa e alta coercividade), contribuição relativa (%), SMRI (saturação de magnetização remanente isotérmica, em A/m), log($B_{1/2}$) (campo de meia remanescência, em mT), $B_{1/2}$ (mT) e DP (parâmetro de dispersão, em mT).

Type of material	Component	S-Ratio	Contribution (%)	SIRM (A/m)	Log($B_{1/2}$) (mT)	$B_{1/2}$ (mT)	DP (mT)
Tabacco	1	0.934	97.4	3.80x10^{-2}	1.63	42.7	0.43
	2		2.6	1.00x10^{-1}	3.10	1258.9	0.20
Tabacco Ash	1	0.986	100	1.51	1.62	41.7	0.35
Cigarette filter (used)	1	0.988	68.8	2.20x10^{-2}	1.25	17.8	0.52

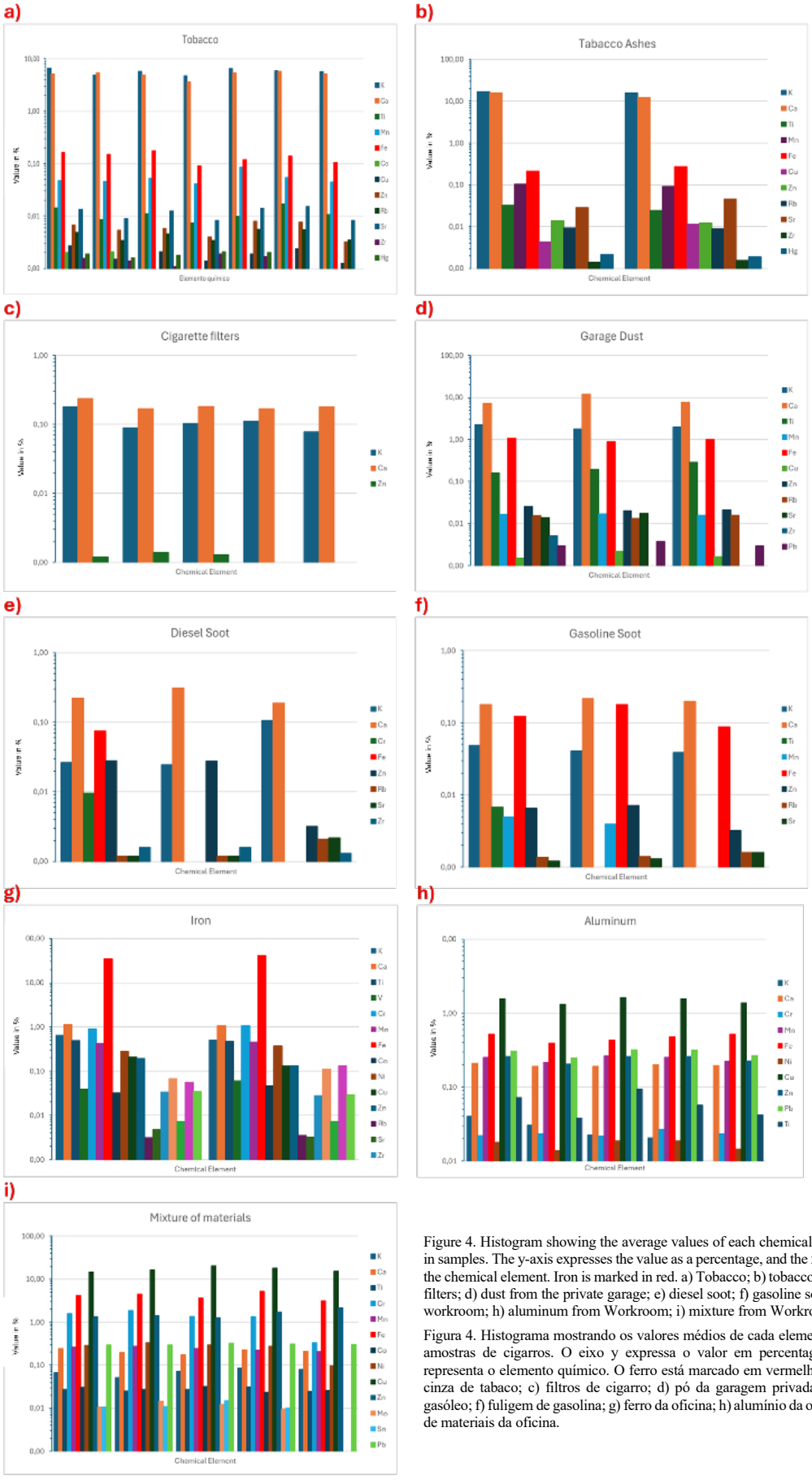

Figure 4. Histogram showing the average values of each chemical element present in samples. The y-axis expresses the value as a percentage, and the x-axis represents the chemical element. Iron is marked in red. a) Tobacco; b) tobacco ash; c) cigarette filters; d) dust from the private garage; e) diesel soot; f) gasoline soot; g) iron from workroom; h) aluminum from Workroom; i) mixture from Workroom.

Figura 4. Histograma mostrando os valores médios de cada elemento presente nas amostras de cigarros. O eixo y expressa o valor em percentagem e o eixo x representa o elemento químico. O ferro está marcado em vermelho. a) Tabaco; b) cinza de tabaco; c) filtros de cigarro; d) pó da garagem privada; e) fuligem de gasóleo; f) fuligem de gasolina; g) ferro da oficina; h) alumínio da oficina; i) mistura de materiais da oficina.

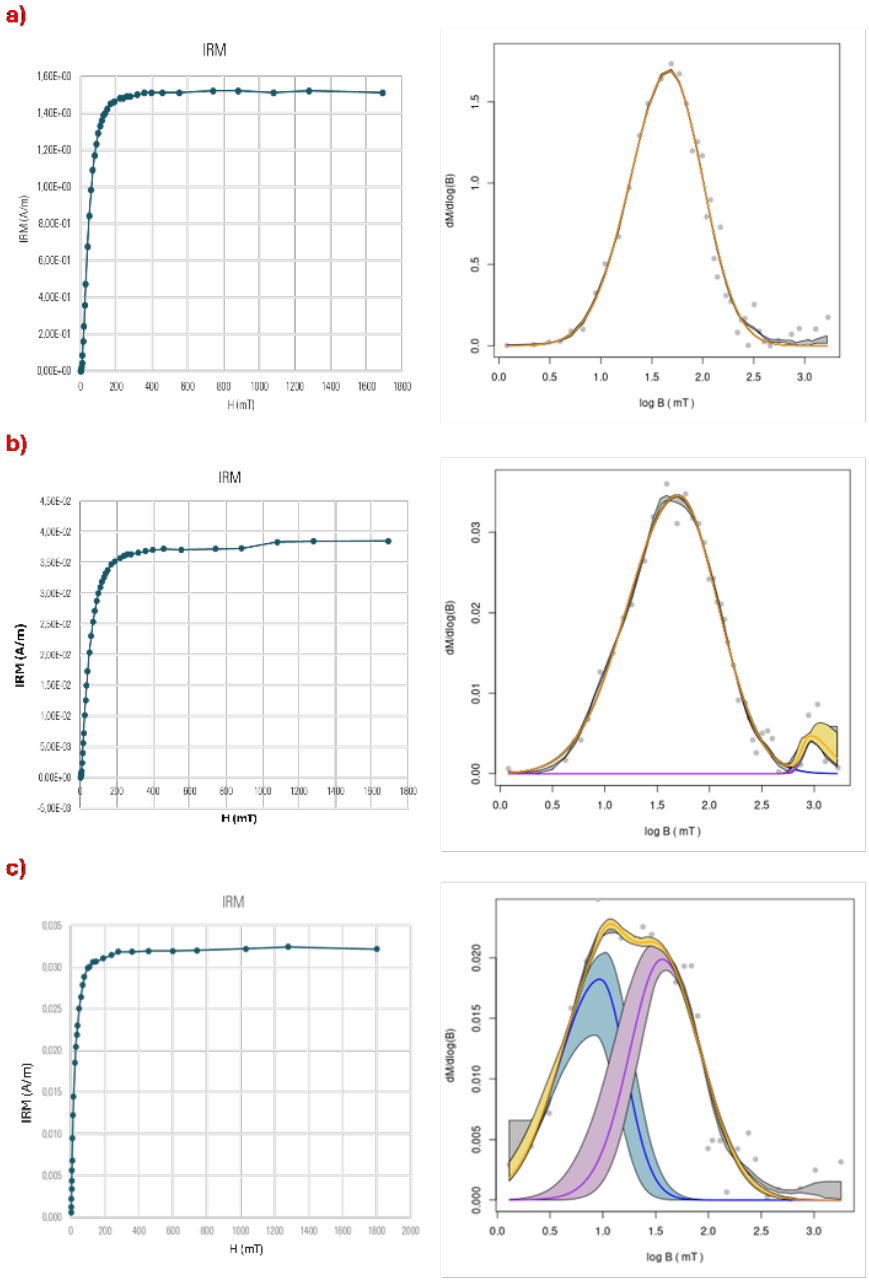

Figure 5. Isothermal Remanent Magnetization of the materials (left) and Max unmix technique (right). a) Tobacco sample; b) ash sample; c) cigarette filter.

Figura 5. Magnetização Remanente Isotérmica dos materiais (direita) e técnica Max unmix (esquerda); a) Amostra de tabaco; b) amostra de cinzas; c) filtro de cigarro.

3.6. Thermomagnetic Curves (K/T)

In this work, we present the thermomagnetic curves corrected for the holder contribution (Fig. 6). The materials chosen for the analyzes of the Thermomagnetic curves (K/T) followed the same criteria as the IRM analyzes also due to the limited number of analytical slots available, as such, the materials chosen were tobacco and tobacco ash.

Regarding the tobacco samples (Fig. 6a), the heating curves do not show a sharp drop at 580 °C. Instead, a slight inflection is observed, suggesting the presence of magnetite (Fe_3O_4), as this corresponds to its Curie temperature. Furthermore, the cooling curve displays an enhancement relative to the heating curve, indicating the formation of a new magnetic phase, likely magnetite, during the heating process.

The tobacco ash results (Figs. 6b, c, d) reveal a subtle inflection near 580 °C, suggesting that magnetite may be present. Notably, a continuous decrease in susceptibility begins at 200 °C, followed by the characteristic drop at 580 °C, typical of magnetite. However, in one specific sample (Fig. 6d), a secondary magnetic transition is observed in the heating curve between 670 °C and 680 °C, indicating the presence of a second magnetic mineral with lower susceptibility, most likely hematite (Fe_2O_3).

4. Discussion

The analysis confirms that several daily materials contain iron-rich particles with distinct magnetic behaviors. Tobacco samples revealed both magnetite (Fe_3O_4) and goethite (FeO(OH)). This indicates that iron in the material occurs not only as an oxide but also as an iron oxyhydroxide, each with distinct magnetic

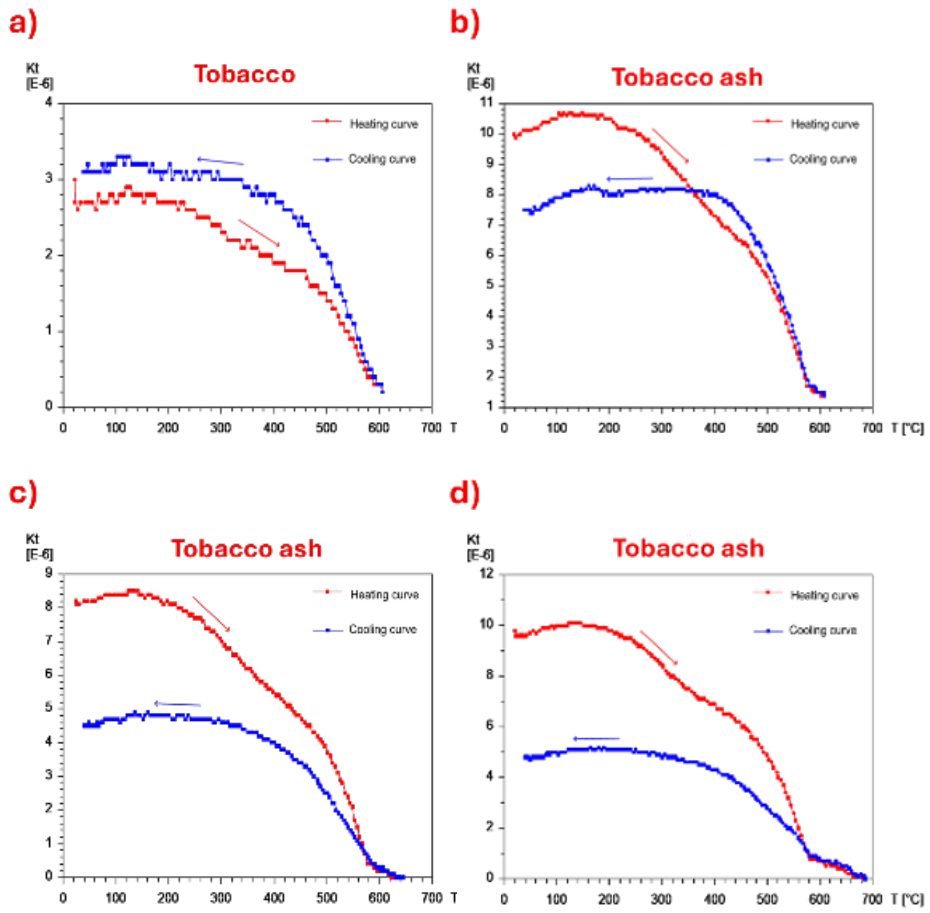

Figure 6. Corrected for the empty furnace thermomagnetic curve of tobacco and tobacco ash samples. a) Tobacco (not corrected); b) tobacco (corrected); c) tobacco ash (not corrected); d) tobacco ash (corrected); e) tobacco ash (not corrected); f) tobacco ash (corrected). Red line – heating curve; Blue line – Cooling curve.

Figura 6. Curva termomagnética corrigida em função da curva termomagnética em forno vazio, das amostras de tabaco e da cinza de tabaco. a) tabaco (não corrigida); b) tabaco (corrigida); c) cinza de tabaco (não corrigida); d) cinza de tabaco (corrigida); e) cinza de tabaco (não corrigida); f) cinza de tabaco (corrigida). Linha vermelha – curva de aquecimento; Linha azul – Curva de arrefecimento.

properties and coercivities. Additionally, in one sample, the cooling curve shows higher values than the heating curve, suggesting the formation of a new magnetic phase (magnetite) likely produced through the thermal transformation (Usman *et al*., 2013) of goethite.

Combustion changes the physical and chemical properties of tobacco, and this is proven by the results of the ashes that exhibited stronger ferromagnetic signals and higher iron concentrations than unburned tobacco, indicating thermal transformation of goethite into magnetite. These ultrafine particles < 2 μm of magnetite and other components pose inhalation risks due to their ability to penetrate pulmonary alveoli.

This mineralogical shift is further supported by the geochemical data obtained through XRF analysis. The concentration of Fe increased significantly from raw tobacco to its combustion by-products, rising from a mean value of 1353 ppm in the pre-combustion stage to 2450 ppm in the tobacco ashes. This enrichment in iron, coupled with the thermal synthesis of magnetite, explains the transition from a paramagnetic to a strong ferromagnetic behavior. Filters demonstrated contrasting behaviors, unused filters were diamagnetic, while used filters became paramagnetic, reflecting retention of iron-bearing particles from smoke. Although XRF did not detect Fe in filters samples, magnetic susceptibility and IRM confirmed the magnetite presence, suggesting concentrations below detection limits. This highlights the role of filters as partial traps for combustion-derived particles, only allowing the fine particles to enter the respiratory system.

Garage dust contained, in addition to other particles, sub-rounded particles with high Fe concentrations and ferromagnetic responses, consistent with magnetite. The morphology of particles indicates transport from external sources such as tires or shoes, underscoring the environmental persistence of magnetic particles but their size could be easily inhaled during breathing. These findings are supported by XRF analysis, which recorded a concentration of 9861 ppm of Fe, correlating the high metal content with the intense magnetic signal observed.

Industrial paints and hair dyes, in contrast, showed diamagnetic or weak paramagnetic behavior, which indicates none, or only a few, minerals that have iron (*e.g.*, biotite) probably used in pigments, excluding significant iron oxide presence and thus posing minimal risk.

Fuel soot analyses revealed micrometric particles with paramagnetic responses. Geochemical data confirms this behavior and shows that diesel soot (1302 ppm) contains nearly double the iron concentration of gasoline soot (757 ppm). Diesel soot consistently contained higher Fe concentrations and stronger susceptibility than gasoline soot, suggesting greater toxicological risk due to iron oxide content. Both samples contain iron particles large enough to enter the bloodstream and are also constantly released, since cars are in constant circulation in the city.

Metal scraps and the iron samples exhibited ferromagnetic behavior, with large, oxidized particles capable of fragmenting into ultrafine inhalable dust, raising occupational health concerns. XRF analysis revealed extreme Fe concentrations, reaching the mean value of 378953 ppm, being the highest value recorded in this study, for the iron-based samples and 42291 ppm in mixture samples. These geochemical results explain the saturation of the magnetic signals and underscore the high density of metallic particles in these environments.

Overall, the findings demonstrate that magnetic particles originated from specific everyday materials can be incorporated into human tissues via inhalation, with accumulation in organs such as the heart, brain, and lungs (Marques, 2013; Sant'Ovaia *et al.*, 2015). Unlike studies focusing on general atmospheric pollution, our results pinpoint individual sources of exposure, showing how common activities contribute to the buildup of iron-rich matter. Such accumulation may trigger oxidative stress and inflammatory responses, contributing to respiratory, cardiovascular, and neurological disorders. The study emphasizes the importance of monitoring ultrafine ferromagnetic particles in urban and industrial environments.

5. Conclusion

The combined use of microscopy (optical and SEM-EDS), geochemical analyses (XRF), and magnetic measurements (magnetic susceptibility, IRM, and thermomagnetic curves) enabled a robust characterization of iron oxides in non-geological materials of everyday use. Tobacco, ashes, filters, garage dust, fuel soot, and metal scraps all contained ferromagnetic particles, primarily magnetite, often within the micro- to submicrometric range (~2µm). These ultrafine particles are small enough to penetrate pulmonary alveoli and enter the bloodstream, raising concerns about respiratory, cardiovascular, and neurological effects. In contrast, industrial paints and hair dyes exhibited diamagnetic or weak paramagnetic behavior, excluding significant iron oxide presence and thus posing minimal risk.

The results highlight that combustion processes and industrial activities generate magnetically active particles capable of persisting in the environment and accumulating in human tissues. Their bioactivity, potential oxidative stress and inflammatory responses underscore the importance of monitoring fine iron-rich particles in urban and occupational settings. Future research should expand the range of materials studied and investigate pathways of iron (Fe) oxide accumulation in human organs. Other elements of potential importance for further study include lead (Pb), chromium (Cr), nickel (Ni), cobalt (Co), cadmium (Cd), and manganese (Mn), due to their documented associations with carcinogenic effects and severe systemic toxicities upon chronic exposure, aiming to better understand their toxicological implications.

Acknowledgements

The authors thank Mário Moreira for the helpful guidance in paleomagnetism and explanations during the IRM and K/T analysis carried out in the Paleomagnetism Laboratory from Instituto Dom Luiz. We would like to express our sincere gratitude to the anonymous reviewer, to Tania Molaches, and to the editor of Comunicações Geológicas for their valuable comments and suggestions, which greatly contributed to improving this article.

Funding

The authors acknowledge the financial support provided to the Institute of Earth Sciences (ICT) through the multi-annual funding contract with the Foundation for Science and Technology (FCT), under project UID/04683/2025 with the DOI https://doi.org/10.54499/UID/04683/2025. Cláudia Cruz is a researcher hired under the Individual Scientific Employment Stimulus Program, reference 2023.07410.CEECIND (Fundação para a Ciência e a Tecnologia − Portugal).

References

Baker, R. R., 1987. A review of pyrolysis studies to unravel reaction steps in burning tobacco. *J. Analytical and Applied Pyrolysis*, **11:** 555-573. https://doi.org/10.1016/0165-2370(87)85054-4.

Baliga, V. L., Miser, D. E., Sharma, R. K., Thurston, M. E., Chan, W. G., Hajaligol, M. R., 2003. Physical characterization of the cigarette coal: part 1- smolder burn. *J. Analytical and Applied Pyrolysis,* **68-69**: 443-465. https://doi.org/10.1016/S0165-2370(03)00081-0.

Calderón-Garcidueñas, L., González-Maciel, A., Mukherjee, P. S., Reynoso-Robles, R., Pérez-Guillé, B., Gayosso-Chávez, C., Torres-Jardón, R., Cross, J. V., Ahmed, I. A. M., Karloukovski, V. V., Maher, B. A., 2019. Combustion-and friction-derived magnetic air pollution nanoparticles in human hearts. *Environmental Research*, **176**, 108-567. https://doi.org/10.1016/j.envres.2019.108567.

Cohen, D., 1973. Ferromagnetic contamination in the lungs and other organs of the human body. *Science*, **180**(4087): 745-748. https://doi.org/10.1126/science.180.4087.745.

Dezube, R., 2023. *Respiratory System Defense Mechanisms*. MSD Manual Consumer Version. Available at: www.msdmanuals.com. [Accessed January 2025].

Fischer, P., Götz, M. E., Danielczyk, W., Gsell, W., & Riederer, P., 1997. Blood transferrin and ferritin in Alzheimer's disease. *Life sciences*, **60**(25): 2273-2278. https://doi.org/10.1016/S0024-3205(97)00282-8.

Gunawan, C., Fleming, C., Irga, P. J., Wong, R. J., Amal, R., Torpy, F. R.,Galzan, S. M., McGrath, K. C., 2024. Neurodegenerative effects of air pollutant Particles: Biological mechanisms implicated for Early-Onset alzheimer's disease. *Environment International,* **185**: 108512. https://doi.org/10.1016/j.envint.2024.108512.

Haacke, E. M., Cheng, N. Y., House, M. J., Liu, Q., Neelavalli, J., Ogg, R. J., Khan, A., Ayaz, M., Kirsch W., Obenaus, A., 2005. Imaging iron stores in the brain using magnetic resonance imaging. *Magnetic resonance imaging*, **23**(1): 1-25. https://doi.org/10.1016/j.mri.2004.10.001.

Ikeda, M., 2001. Iron overload without the C282Y mutation in patients with epilepsy. *Journal of Neurology, Neurosurgery & Psychiatry*, ***70***(4): 551-553. https://doi.org/10.1136/jnnp.70.4.551.

Kirschvink, J. L., Kobayashi-Kirschvink, A., Diaz-Ricci, J. C., Kirschvink, S. J., 1992. Magnetite in human tissues: a mechanism for the biological effects of weak ELF magnetic fields. *Bioelectromagnetics*, **13**(S1): 101-113. https://doi.org/10.1002/bem.2250130710.

Loeffler, D. A., Connor, J. R., Juneau, P. L., Snyder, B. S., Kanaley, L., DeMaggio, A. J., Brickman, C. M., LeWitt, P. A., 1995. Transferrin and iron in normal, Alzheimer's disease, and Parkinson's disease brain regions. *Journal of Neurochemistry*, **65**(2): 710-716. https://doi.org/10.1046/j.1471-4159.1995.65020710.x.

Maher, B. A., 2019. Airborne magnetite-and iron-rich pollution nanoparticles: potential neurotoxicants and environmental risk factors for neurodegenerative disease, including Alzheimer's disease. *Journal of Alzheimer's Disease*, **71**(2): 361-375. https://doi.org/10.3233/JAD-190204.

Marques, G. M., 2013. *Estudo das Propriedades Magnéticas de Tecidos Humanos* (Master's thesis, Universidade do Porto (Portugal)). 57.

Maxbauer, D. P., Feinberg, J. M., Fox, D. L., 2016. MAX UnMix: A web application for unmixing magnetic coercivity distributions. *Computers & Geosciences*, **95**: 140-145. https://doi.org/10.1016/j.cageo.2016.07.009.

Robertson, D. J., France, D. E., 1994. Discrimination of remanence-carrying minerals in mixtures, using isothermal remanent magnetisation acquisition curves. *Physics of the Earth and Planetary interiors,* **82**(3-4): 223-234. https://doi.org/10.1016/0031-9201(94)90074-4.

Samet, J. M., Dominici, F., Curriero, F. C., Coursac, I., Zeger, S. L., 2000. Fine particulate air pollution and mortality in 20 US cities, 1987–1994. *New England journal of medicine*, **343**(24): 1742-1749. https://doi.org/10.1056/NEJM200012143432401.

Sant'Ovaia, H., Marques, G., Santos, A., Gomes, C., Rocha, A., 2015. Magnetic susceptibility and isothermal remanent magnetization in human tissues: A study case. *Biometals, **28***: 951-958. https://doi.org/10.1007/s10534-015-9879-z.

Simovich, M., Hainsworth, L. N., Fields, P. A., Umbreit, J. N., & Conrad, M. E., 2003. Localization of the iron transport proteins mobilferrin and DMT-1 in the duodenum: The surprising role of mucin. American journal of hematology, **74**(1): 32-45. https://doi.org/10.1002/ajh.10383.

Thompson, R., Oldfield, F., 1986. Magnetic properties of natural materials. *Environmental magnetism*. Springer Netherlands, 21-38. http://doi.org/10.1007/978-94-011-8036-8.

Umbreit, J. N., Conrad, M. E., Hainsworth, L. N., Simovich, M., 2002. The ferrireductase paraferritin contains divalent metal transporter as well as mobilferrin. *American Journal of Physiology-Gastrointestinal and Liver Physiology*, **282**(3): 534-539. https://doi.org/10.1152/ajpgi.00199.2001.

Usman, M., Abdelmoula, M., Faure, P., Ruby, C., Hanna, K., 2013. Transformation of various kinds of goethite into magnetite: Effect of chemical and surface properties. *Geoderma*, **197**: 9-16. https://doi.org/10.1016/j.geoderma.2012.12.015.